Nonlinear stability of traffic models and the use of Lyapunov vectors for estimating the traffic state

Luigi Palatella,[1,2] Anna Trevisan,[3] and Sandro Rambaldi[1]
[1]*Centro Interdipartimentale CIG L. Galvani Università di Bologna, Via Selmi n. 3, Bologna, Italy*
[2]*Istituto di Scienze dell'Atmosfera e del Clima del CNR, U.O.S. di Lecce, Str. Prov. Lecce-Monteroni km 1200, Lecce, Italy*
[3]*Istituto di Scienze dell'Atmosfera e del Clima del CNR, via P. Gobetti 101, Bologna, Italy*
(Received 26 March 2013; published 1 August 2013)

Valuable information for estimating the traffic flow is obtained with current GPS technology by monitoring position and velocity of vehicles. In this paper, we present a proof of concept study that shows how the traffic state can be estimated using only partial and noisy data by assimilating them in a dynamical model. Our approach is based on a data assimilation algorithm, developed by the authors for chaotic geophysical models, designed to be equivalent but computationally much less demanding than the traditional extended Kalman filter. Here we show that the algorithm is even more efficient if the system is not chaotic and demonstrate by numerical experiments that an accurate reconstruction of the complete traffic state can be obtained at a very low computational cost by monitoring only a small percentage of vehicles.

DOI: 10.1103/PhysRevE.88.022901 PACS number(s): 05.45.Gg, 89.40.−a, 05.45.Jn

I. INTRODUCTION

New information technologies allow direct measures of individual mobility behavior [1–3], opening the concrete possibility to build up a new class of models able to describe and also to predict the traffic dynamics. In turn, the mobility governance could be more effective, especially the ability to control and prevent critical situations such as congestions [4–6]. In Italy, for example, this technology is widespread and a sample of 3% for the whole vehicles population has an Octo Telematics GPS system for insurance reasons. Any car is associated with an ID number, so that it is possible to follow its motion over a long period of time. Each observation gives position, velocity, and distance covered from the previous observation together with the signal quality [7]. The data sample is constituted by trajectory points at a space interval of about 2 km. The data suffer from the GPS's limited precision, in particular when the GPS loses the satellite signal. When the signal quality is good, the time precision of the recorded data is perfect, whereas the space precision is of the order of 10 m, often sufficient to localize the vehicle on the road in a unique way.

The aim of our research work is to use these data to reconstruct a correct state of the full system using only this 3% of monitored vehicles and all the physical relations known. The problem of estimating the state of an evolving system from an incomplete set of noisy observations and the approximate knowledge of the evolution equations is the central theme of the classical estimation and control theory [8]. One of its most significant domains of application is numerical weather and oceanic prediction, where the problem is usually referred to as data assimilation and the aim is to provide an accurate estimate of the initial state, the *analysis*, for prediction models. The analysis is obtained by merging, under some optimal criteria, the information coming from the model and the observations. In this paper, we will use an assimilation algorithm recently developed by the authors for geophysical applications, in conjunction with a traffic model introduced by Refs. [9,10] and referred to in the literature as the *optimal velocity* (OV) model. We will perform simulation experiments with a realistic observation system to estimate the full traffic state from incomplete data.

In the so-called "microscopic" traffic models, the dynamic equations governing the motion of each individual vehicle are prescribed in terms of their mutual interaction. In the OV model, vehicles tend to maintain a safe speed that depends on the distance from the vehicle ahead. Mathematically, the model consists of second-order differential equations for the positions of vehicles. In its simplest version, the OV model describes the motion of vehicles in a single-lane road stretch or a circular circuit, but it can be used in more complex road networks.

Most studies have investigated the dynamical properties of the OV model by means of numerical simulation and simple analytical arguments, such as linear stability analysis of equilibrium solutions. Homogeneous flow is the steady-state solution where all cars proceed at constant speed and have the same relative distance. For car densities larger than a critical value, traffic congestion spontaneously occurs when homogeneous flow is perturbed. Numerical solutions show typical stop-and-go patterns moving backward with velocity v_B, stop-fronts connecting high velocity to almost zero velocity, and go-fronts connecting almost zero velocity to high velocity. For a review see Refs. [11,12].

Closed trajectories in the form of an analytical solution for congested flow were obtained by Ref. [13]. The time delay T and the backward velocity v_B of repetitive patterns could be related to the model parameters. The authors of Ref. [14] observed that since the stop-and-go waves propagate at about the same speed, the motion of a vehicle is approximately periodic in time because it encounters the same traffic pattern for each circuit, albeit shifted according to the wave speed. This observation motivated their study of periodic orbits in an OV model (that takes into account reaction-time delay T of drivers). In addition, they studied the stability of periodic orbits by examining the structure of Floquet eigendirections. Results showed that unstable structures of periodic orbits take place near the fronts, indicating that any eventual instability is due to the motion of the fronts.

The first goal of the present work is to study the stability of OV models with tools of dynamical systems theory, based on the computation of Lyapunov exponents and vectors that

are the natural generalization for aperiodic orbits of Floquet exponents and eigenvectors for periodic orbits [15]. The second goal of the study is to test, in an idealized context, assimilation algorithms that can be applied to traffic models in real situations.

State estimation for a traffic flow refers to estimating all traffic variables at the current time instant by assimilating available real-time traffic measurements and has been identified as an important task for traffic control already in the 1970s [16]. A number of research works proposed estimation algorithms that were based on Kalman filtering (KF) [17] and its extensions for nonlinear systems, the extended Kalman filter (EKF) (see, e.g., Ref. [8]).

The Kalman filter has been applied in the field of traffic dynamics starting with early applications of traffic state estimation in traffic surveillance systems for short interdetector distances by Refs. [18–22]. In these and later investigations, e.g., Refs. [23,24], short freeway sections were considered (for a review, see Ref. [25]). The applied models were relatively simple. Later approaches started using more comprehensive dynamic traffic flow models, including longer freeway stretches (2–4 km) [26,27]. Further investigations elaborated some technical details based on previously proposed basic ideas [28,29] to end up with more comprehensive and recent studies [30–32].

All these works are based on the class of models known in the literature as *macroscopic* traffic models [11]. The choice of macroscopic instead of microscopic models was most likely dictated by the following technical reason: the use of the Kalman filter becomes prohibitive for real-time applications due to its computational burden when the model has a large number of degrees of freedom. In the present work, we propose to use an algorithm that overcomes this difficulty because it produces the same results as the EKF but at a very low computational cost; the algorithm is, therefore, suitable for applications to microscopic models.

The data assimilation algorithm belongs to the family that goes under the name of assimilation in the unstable subspace (AUS) and we will apply it to the OV model to reconstruct the traffic state. The AUS formulation was developed by the authors of the present work in two different well-known contexts of state estimation theory [8]. The first is the variational approach to the estimation problem, and in this context the algorithm, developed within the well-established four-dimensional variational assimilation (4DVar) [33] context is referred to as 4DVar-AUS [34]. The formulation of the algorithm in the context of nonlinear Kalman filtering, and in particular of the EKF, is referred to as EKF-AUS [35]. The AUS-type algorithms [34,36–38] exploit the nonlinear stability properties of the forecasting model in their formulation and use the Lyapunov vectors with positive and zero exponents to define the subspace where the analysis solution must be confined. This leads to an efficient and computationally inexpensive way of reducing errors that grow due to sensitivity to initial conditions, as shown in previous applications to atmospheric and oceanic models [39].

In the present study, we will consider the dynamics of vehicles in a circular circuit to be described by the OV model; we then apply the EKF-AUS algorithm to perform observation system simulation experiments, i.e., by making use of synthetic measurements of the vehicles' position and velocity with observation errors compatible with the present technology. The number of observed vehicles is varied and can be as small as dictated by the presently available number of monitored cars. The aim is testing the ability of the algorithm to reconstruct the complete microscopic traffic state, i.e., to estimate the position and velocity of all vehicles, when the number of observed vehicles is much smaller than the total number of vehicles present in the domain, before it can be used for practical applications.

The outline of the paper is the following: in Sec. II we describe the OV model; in Sec. III we study its stability properties while in Sec. IV we describe the EKF-AUS algorithm; in Sec. V we show the numerical results while the conclusions are shown in Sec. VI.

II. THE OPTIMAL VELOCITY MODEL

The model, referred to in the literature as microscopic OV traffic model is a deterministic dynamical system, where the motion of individual vehicles is described by second-order ordinary differential equations:

$$\begin{aligned} \dot{s}_i(t) &= v_i(t) \\ \dot{v}_i(t) &= -\beta\{v_i(t) - v_{\mathrm{opt}}[s_{i-1}(t) - s_i(t)]\}, \end{aligned} \tag{1}$$

where $s_i(t), v_i(t)$ indicate position and velocity of the ith vehicle. The driver tends to maintain a safe distance so that optimal velocity function, $v_{\mathrm{opt}}(x)$ depends on the corresponding instantaneous distance headway, $s_{i-1}(t) - s_i(t)$. For explicit calculations, it is necessary to specify a particular function form of $v_{\mathrm{opt}}(x)$

The following choice is made for the optimal velocity function [40],

$$v_{\mathrm{opt}}(x) \equiv \begin{cases} 0 & \text{if } x < d \\ v_\infty[1 - x^{-a}]^m & \text{if } x \geqslant d, \end{cases} \tag{2}$$

and for the numerical values of parameters,

$$a = 0.75, \quad m = 1, \quad v_\infty = 1, \quad d = 1. \tag{3}$$

An ad-hoc choice of β is made so that cars cannot overtake each other:

$$\beta \equiv \begin{cases} 5 & \text{if } v_i(t) - v_{\mathrm{opt}}[s_{i-1}(t) - s_i(t)] > 0 \\ & \wedge\, s_{i-1}(t) - s_i(t) < 0.3\, d \\ \beta_0; & \text{otherwise}, \end{cases} \tag{4}$$

where β_0 is a parameter that can be tuned.

The choice of boundary conditions has important consequences on the resulting dynamics and on its stability. Periodic boundary conditions are used to simulate traffic in a circular road with a fixed number of vehicles in the circuit. Empirical boundary conditions are used to prescribe the inflow of vehicles, obtained by adding a new vehicle at the beginning of a highway stretch (as it enters from the left) with free outflow of vehicles at its (right) end. In such a case, the total number of vehicles is variable and is determined by the internal dynamics and by the, possibly stochastic, prescription of their inflow.

To perform the data assimilation procedure, we need to study the time evolution of the small perturbations of the

analysis trajectories. To this purpose, we evaluate the Jacobian of the differential equations given by Eq. (1). To numerically optimize the calculation we study the time evolution of a number of vectors equal to the number of perturbations m used in the EKF-AUS algorithm. This number is considerably lower than the number of degrees of freedom of the system. The vectors evolve according to the linear tangent model (LTM) given by

$$\frac{d\mathbf{X}}{dt} = \mathcal{J}\mathbf{X}, \tag{5}$$

where $\mathbf{X}$ is a $2N \times m$ matrix whose columns are the perturbation vectors and the Jacobian $\mathcal{J}$ is given by

$$\mathcal{J}_{ij} = \frac{\partial \dot{x}_i(t)}{\partial x_j}, \tag{6}$$

and the state vector position and velocity variables are organized so that the transpose of $\mathbf{x}$ is given by:

$$\mathbf{x}^T = \{s_1, s_2, \ldots, s_N, v_1, v_2, \ldots, v_N\}, \tag{7}$$

where N is the number of cars. Recalling Eq. (1), we have

$$\mathcal{J} = \begin{pmatrix} \mathbf{0} & \mathbf{I} \\ \beta\mathcal{V} & -\beta\mathbf{I} \end{pmatrix}, \tag{8}$$

where $\mathbf{I}, \mathbf{0}$ are the identity and null $N \times N$ matrix, respectively, while

$$\mathcal{V}_{ij} = \begin{cases} -\left.\frac{dv_{\rm opt}(s)}{ds}\right|_{s=s_{j-1}-s_j} & \text{if } i = j \\ \left.\frac{dv_{\rm opt}(s)}{ds}\right|_{s=s_{j-1}-s_j} & \text{if } i = j+1, \end{cases} \tag{9}$$

where we have made use of the fact that

$$\frac{\partial v_{\rm opt}(s_{i-1} - s_i)}{\partial s_i} = -\frac{\partial v_{\rm opt}(s_{i-1} - s_i)}{\partial s_{i-1}}. \tag{10}$$

For simplicity, we have neglected the dependance of β on s_i and v_i that occurs in the particular condition of a car that is about to collide with the car ahead and for particular values of s_i e v_i. The matrix $\mathbf{X}$ has a number of columns, m, equal to the number of perturbation vectors needed for a specific application. When studying the stability of the OV model (see Sec. III) m is equal to the number of Lyapunov exponents and vectors that one wishes to estimate. In the state estimation problem, m is equal to the number of perturbations needed by the filter; as reviewed in Sec. IV, the EKF-AUS algorithm uses a number of perturbations approximately equal to the dimension of the unstable and neutral subspace, with a very significant reduction of computational burden compared to that of the full EKF.

III. STABILITY STUDY OF THE OV MODEL

The stability of an aperiodic orbit is studied by considering the evolution along the flow of infinitesimal perturbations. The dynamics is described by the tangent linear equations and defines the tangent space of the nonlinear trajectory. Lyapunov vectors can be considered the generalization of the eigenmodes of a fixed point and Floquet vectors of a periodic orbit. Lyapunov vectors are norm independent and covariant with the dynamics; i.e., a vector associated to a given exponent at a given point is mapped by the tangent linear equations into its image at any subsequent point along the nonlinear trajectory [15,36,41,42]. The span of Lyapunov vectors with positive, null, and negative exponents defines the unstable, neutral end stable manifolds of the system. Because, in general, Lyapunov vectors are not orthogonal to one another, their numerical computation is not straightforward. Computing the subspaces spanned by a given number of Lyapunov vectors is obtained efficiently by performing recurrent orthonormalizations [44], but computing the individual vectors themselves requires the use of complex numerical algorithms that involve the intersections of subspaces obtained by forward and backward orthonormalization, i.e., proceeding in direct or reverse order with respect to the order of the exponents (see, e.g., Ref. [15]). This procedure is not computationally affordable for high-dimensional systems: for a review of recently developed algorithms for the computation of Lyapunov vectors of high-dimensional systems see Ref. [43].

The stability analysis performed with the algorithm of Ref. [44] shows that the OV model is not chaotic. Figures 1 and 2 show the time average of the Lyapunov exponents. In Fig. 1, the Lyapunov exponents become negative except for two. In Fig. 2, where the time average starts from $t > 5 \times 10^6$, only one exponent remains positive, while the second one is very close to zero. The OV model is autonomous so it must have at least one null Lyapunov exponent associated to the vector that is tangent to the trajectory in the phase-space. Moreover, the case of periodic boundary condition that is treated in this paper has an exact translation symmetry given by $s_i(t) \to s_i(t) + \tilde{L}$, where $\tilde{L}$ does not depend on i. This implies that the system has at least another null Lyapunov exponent. For this reason, even if it is very difficult from the numerical standpoint to achieve convergence, we conclude that the system is not chaotic.

It is worth noticing that the question of the computation of a null Lyapunov exponent is quite delicate. As with all zero

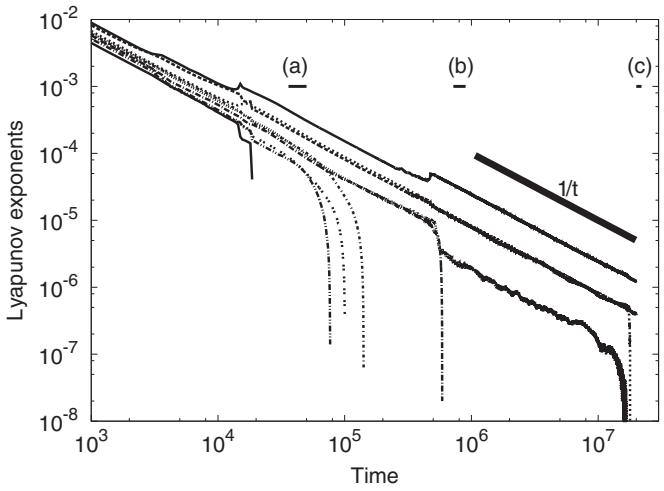

FIG. 1. Calculation of the Lyapunov exponents according to the algorithm [44] as a function of time over which the exponents are averaged. $N = 150, \beta = 0.4, L = 200$. The three short time intervals that will be used in the assimilation experiments are shown in the figure and are labeled (a), (b), and (c). The top thick line labeled as $1/t$ is plotted for comparison with the asymptotic behavior of the exponents.

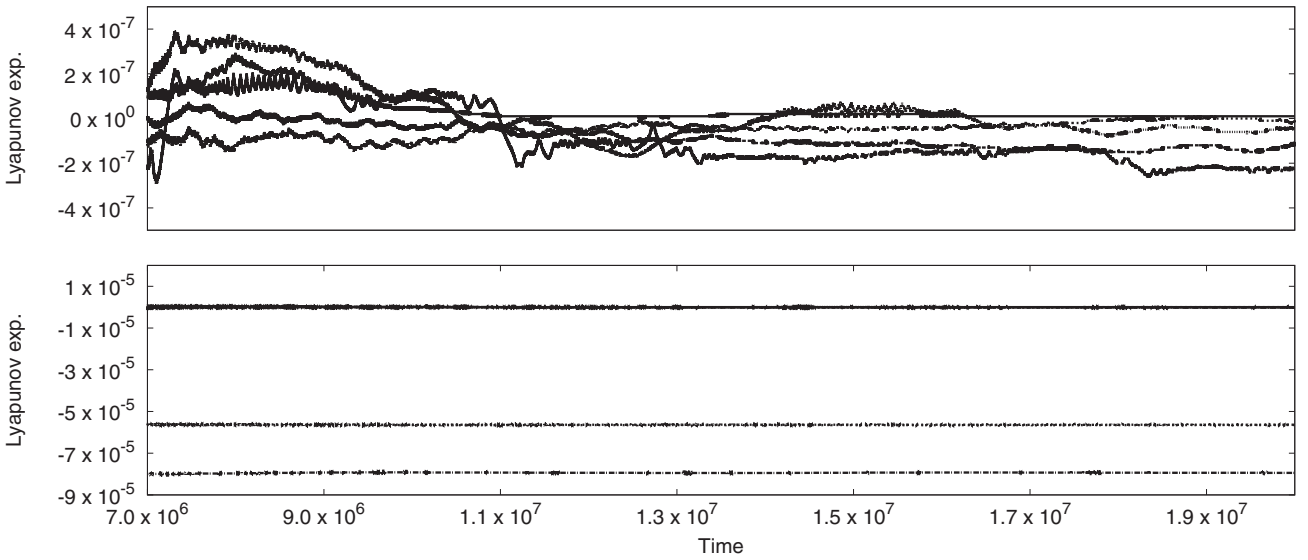

FIG. 2. Calculation of the Lyapunov exponents according to the algorithm [44] as a function of time over which the exponents are averaged. $N = 150$, $\beta = 0.4$, $L = 200$. Different from Fig. 1, here the averaging procedure starts at $t = 5 \times 10^6$.

measurements, there is always a numerical problem in stating that a floating double precision number is actually zero. This problem does not come from round-off errors but from the fact that the algorithm used to calculate Lyapunov exponents leads to slow convergence to zero in the nonchaotic case.

This is because the Lyapunov exponents are obtained as the ratio between the logarithm of the amplification factor of the perturbation during a time interval and the time interval itself. Perturbations associated with zero exponents, as is the case for the perturbation tangent to an aperiodic orbit and for all perturbations of a stable periodic orbit, do not grow asymptotically; consequently, the logarithm of their amplification factor divided by time leads to a $1/t$ convergence to zero. For this reason, a typical rule of thumb to state that the Lyapunov exponent is zero is to observe a $1/t$ behavior in log scale. To stress this point, we added a $1/t$ decay curve in Fig. 1 to show that this is in fact the case.

The reader may ask what is the error that should be assigned to the estimate of the Lyapunov exponent. A reasonable criterion is to evaluate the inverse of the average time (in our case 10^{-7}) as an upper limit. Consequently, if for a time range of 10^7 we observe a $1/t$ decay in log-log scale and if the averaged value of the leading Lyapunov exponent is less than 10^{-7}, as happens in our case, we can conclude that the leading exponent is zero within a numerical approximation of 10^{-7}.

The implications of this result for the application of assimilation algorithms to the OV model are discussed in the next section.

IV. STATE ESTIMATION IN THE OV MODEL THROUGH THE EKF-AUS ALGORITHM

In the present work, we consider the application to the OV traffic model of an algorithm developed by the authors for geophysical data assimilation, the EKF-AUS. The essence of AUS is the formal implementation of a simple concept. If a dynamical system has a tangent space with central, stable, and unstable manifolds, when updating the state by the use of new observations it is sufficient to make corrections only in the unstable and neutral directions where small errors in the previous state estimate tend to amplify. This is because, in the long run, errors in the stable directions naturally tend to be damped by the system dynamics and making corrections in such directions can only artificially introduce observational errors in the state estimate [34].

An important observation is that the EKF-AUS algorithm automatically selects the unstable directions so that the only information that must be externally provided is the estimate (or a reasonable initial overestimate) of their number. This estimate is used to prescribe the number of initially random perturbations; in the course of filter iterations, these perturbations will align along the most unstable directions of the system, the subspace where the update of the state is confined. In practice, starting from a sufficiently large number m_0 of perturbations, if the (estimated) errors associated with the various directions tend to zero, except for a number $m < m_0$, then the value of m will coincide with the number of unstable and neutral directions. This is precisely what happens if the number and accuracy of the observations is such that the filter does not diverge and the errors are sufficiently small that their dynamical evolution is virtually linear. In the presence of small nonlinearities in the error dynamics, in practical applications it is sufficient to use a number of perturbations a few units larger than m [34,35].

The EKF-AUS algorithm is derived from a *square-root* implementation of the EKF, and if a number m of perturbations equal to the total number of degrees of freedom of the system is used the EKF equations are recovered. The authors of Ref. [35] have shown that the solution of the full EKF collapses to the EKF-AUS solution because in the long run the rank of error covariance matrices of the EKF becomes equal to the dimension of the unstable and neutral subspace, while the eigenvalues corresponding to the stable directions decay to zero. In many practical applications, the use of the full EKF is prohibitive when the number of degrees of freedom, n is very large as, for example, in weather forecast models ($n > 10^9$). In

such cases, and every time the dimension of the unstable and neutral subspace is much smaller than n, there is an enormous advantage in using the EKF-AUS algorithm.

A. The EKF-AUS algorithm

In the extended Kalman filter, the state evolves according to the full nonlinear equations and the tangent linear operator is used to predict the approximate error statistics. The estimate of the state, referred to as the analysis $\mathbf{x}^a$, is obtained by combining a forecast state $\mathbf{x}^f$ with the possibly incomplete and noisy $2p$-dimensional observations (p is the number of monitored cars) $\mathbf{y}_k^0 = \mathcal{H}(\mathbf{x}_k) + \varepsilon_k^o$ given at discrete times $t_k > t_0$, $k \in \{1,2,...\}$. The observation error ε_k^o is assumed to be Gaussian with zero mean and known $2p \times 2p$ covariance matrix $\mathbf{R}$. $\mathcal{H}$ is the observation operator. The estimate update is given by the analysis equation:

$$\mathbf{x}_k^a = \mathbf{x}_k^f - \mathbf{K}_k \mathcal{H}\left(\mathbf{x}_k^f\right) + \mathbf{K}_k \mathbf{y}_k^o, \tag{11}$$

where $\mathbf{x}_k^f$ is the *forecast* obtained by integrating the model equations from a previous analysis time,

$$\mathbf{x}_k^f = \mathcal{M}\left(\mathbf{x}_{k-1}^a\right), \tag{12}$$

$\mathcal{M}$ being the nonlinear evolution operator. $\mathbf{K}_k$ is the *gain matrix* at time t_k given by

$$\mathbf{K}_k = \mathbf{P}_k^f \mathbf{H}^T \left(\mathbf{H}\mathbf{P}_k^f \mathbf{H}^T + \mathbf{R}\right)^{-1}, \tag{13}$$

where $\mathbf{H}$ is the Jacobian of $\mathcal{H}$. The analysis error covariance update equation is given by

$$\mathbf{P}_k^a = (\mathbf{I} - \mathbf{K}_k \mathbf{H})\mathbf{P}_k^f, \tag{14}$$

and $\mathbf{P}_k^f$, the forecast error covariance, is given by

$$\mathbf{P}_k^f = \mathbf{M}_k \mathbf{P}_{k-1}^a \mathbf{M}_k^T, \tag{15}$$

where $\mathbf{M}$ is the linearized evolution operator associated with $\mathcal{M}$. We have assumed that there is no model error.

We introduce an algorithm that belongs to the family of square-root implementations of the EKF. A reduced version is then obtained from the full rank algorithm. We perform the assimilation in a manifold of dimension m.

At time $t = t_{k-1}$, let the $n \times m$ matrix $\mathbf{X}^a$ be one of the square roots of $\mathbf{P}^a$, namely $\mathbf{P}^a = \mathbf{X}^a \mathbf{X}^{aT}$, and let the columns of $\mathbf{X}^a = [\delta\mathbf{x}_1^a, \delta\mathbf{x}_2^a, ..., \delta\mathbf{x}_m^a]$ be orthogonal. At time $t = t_0$, the vectors $\delta\mathbf{x}_i^a$, $i = 1,2,...,m$ are arbitrary independent initial perturbations. (Here and in the following we drop the time-step subscript from the equations since, unless otherwise stated, all terms refer to the same time step k).

1. The forecast step

In the forecast step, the tangent linear operator $\mathbf{M}$ acts on the perturbations $\mathbf{X}^a$ defined at (analysis) time $t = t_{k-1}$ (other terms in this and the following equations refer to time step $t = t_k$):

$$\mathbf{X}^f = \mathbf{M}\mathbf{X}^a, \tag{16}$$

where $\mathbf{X}^f = [\delta\mathbf{x}_1^f, \delta\mathbf{x}_2^f, ..., \delta\mathbf{x}_m^f]$. The $n \times n$ forecast error covariance matrix,

$$\mathbf{P}^f = \mathbf{X}^f \mathbf{X}^{fT}, \tag{17}$$

can be cast in the form

$$\mathbf{P}^f = \mathbf{E}^f \Gamma^f \mathbf{E}^{fT}, \tag{18}$$

where the m columns of $\mathbf{E}^f$ are obtained by a Gram-Schmidt orthonormalization of the columns of $\mathbf{X}^f$. The $m \times m$ (in general nondiagonal) symmetric matrix Γ^f defined as

$$\Gamma^f = \mathbf{E}^{fT} \mathbf{X}^f \mathbf{X}^{fT} \mathbf{E}^f \tag{19}$$

represents the forecast error covariance matrix, confined to the subspace $\mathcal{S}^m$ of the evolved perturbations. In the standard EKF algorithm ($m = n$), $\mathbf{E}^f$ is $n \times n$ and its columns span the full space. In the reduced form algorithm, $\mathbf{E}^f$ is $n \times m$ and its columns span an m-dimensional subspace $\mathcal{S}^m$ of the entire phase space.

2. The analysis step

Using the definition of $\mathbf{P}^f$ of Eq. (18), the Kalman gain expression becomes

$$\mathbf{K} = \mathbf{E}^f \Gamma^f (\mathbf{H}\mathbf{E}^f)^T [(\mathbf{H}\mathbf{E}^f)\Gamma^f (\mathbf{H}\mathbf{E}^f)^T + \mathbf{R}]^{-1}, \tag{20}$$

and the usual analysis error covariance update, Eq. (14), reads

$$\begin{aligned}
\mathbf{P}^a &= (\mathbf{I} - \mathbf{K}\mathbf{H})\mathbf{E}^f \Gamma^f \mathbf{E}^{fT} = \mathbf{E}^f \Gamma^f \mathbf{E}^{fT} \\
&\quad - \mathbf{E}^f \Gamma^f (\mathbf{H}\mathbf{E}^f)^T [(\mathbf{H}\mathbf{E}^f)\Gamma^f (\mathbf{H}\mathbf{E}^f)^T + \mathbf{R}]^{-1} \mathbf{H}\mathbf{E}^f \Gamma^f \mathbf{E}^{fT} \\
&= \mathbf{E}^f \{\Gamma^f - \Gamma^f \mathbf{E}^{fT} \mathbf{H}^T [(\mathbf{H}\mathbf{E}^f)\Gamma^f (\mathbf{H}\mathbf{E}^f)^T + \mathbf{R}]^{-1} \\
&\quad \times \mathbf{H}\mathbf{E}^f \Gamma^f\} \mathbf{E}^{fT} \\
&\equiv \mathbf{E}^f \Gamma^{a'} \mathbf{E}^{fT}.
\end{aligned} \tag{21}$$

The analysis error covariance matrix $\mathbf{P}^a$ can be written as

$$\mathbf{P}^a = \mathbf{E}^f \Gamma^{a'} \mathbf{E}^{fT} = \mathbf{E}^f \mathbf{U} \Gamma^a \mathbf{U}^T \mathbf{E}^{fT} \equiv \mathbf{E}^a \Gamma^a \mathbf{E}^{aT}, \tag{22}$$

where the columns of the $(m \times m)$ orthogonal invertible matrix $\mathbf{U}$ are the eigenvectors of the symmetric matrix $\Gamma^{a'} = \mathbf{U}\Gamma^a \mathbf{U}^T$ (to numerically obtain the eigenvalues and the eigenvectors of $\Gamma^{a'}$ we use the power iterations method) and $\Gamma_a = \mathrm{diag}[\gamma_i^2]$ is diagonal. Therefore, the m columns of $\mathbf{E}^a = [\mathbf{e}_1^a, \mathbf{e}_2^a, ..., \mathbf{e}_m^a]$, obtained by

$$\mathbf{E}^a = \mathbf{E}^f \mathbf{U}, \tag{23}$$

span the same subspace $\mathcal{S}^m$ as the columns of $\mathbf{E}^f$. Consequently, the analysis step preserves the subspace $\mathcal{S}^m$. The square root of $\mathbf{P}^a$, written as $\mathbf{P}^a = \mathbf{E}^a \Gamma^a \mathbf{E}^{aT} \equiv \mathbf{X}^a \mathbf{X}^{aT}$, provides a set of orthogonal vectors:

$$\mathbf{X}^a = \mathbf{E}^a (\Gamma^a)^{1/2}. \tag{24}$$

The columns of

$$\mathbf{X}^a = \left[\gamma_1 \mathbf{e}_1^a, \gamma_2 \mathbf{e}_2^a, ..., \gamma_m \mathbf{e}_m^a\right] = \left[\delta\mathbf{x}_1^a, \delta\mathbf{x}_2^a, ..., \delta\mathbf{x}_m^a\right] \tag{25}$$

are the new set of perturbation vectors defined after the analysis step at time t_k that enter the forecast step Eq. (16) at the next time step t_{k+1}. Their amplitude is consistent with the analysis error covariance in the subspace $\mathcal{S}^m$.

Notice that, as in other Kalman square-root filters, with the introduction of $\mathbf{E}^a$ and $\mathbf{E}^f$, forming the full forecast and analysis error covariance matrices can be avoided. The analysis equation is the usual Eq. (11) with $\mathbf{K}$ given by Eq. (20). When $m = n$, $\mathbf{K}$ is the usual Kalman gain. In EKF-AUS ($m = N^+ + N^0$) the analysis increment is confined to the subspace $\mathcal{S}^m$ spanned by the m columns of $\mathbf{E}^f$ in view of the form of $\mathbf{K}$.

V. NUMERICAL RESULTS

We perform the numerical experiments in the perfect model scenario. This means that a single realization of the model evolution, i.e., a trajectory belonging to its attractor, is considered to represent the *truth*. Parallel to the *truth* trajectory, another trajectory, estimate of the true state evolution (called the *analysis*) is obtained by repeatedly applying the assimilation algorithm. The estimated state evolves according to the model equations during a time interval τ, then it is subjected to assimilation using as measure the value obtained applying the measurements operator $\mathcal{H}$ to the *truth* state and adding a Gaussian noise with intensity σ_0.

The OV model is run with the following parameter values:

$$\beta = 0.4, \quad N = 150, \quad L = 200, \quad \sigma_0 = 10^{-2}, \\ \tau = 180, \quad v_\infty = 1.0, \tag{26}$$

where L is the length of the periodic domain. The initial condition is a uniform density state with a noise term added to the position. Considering the length of a car plus the minimum distance being of the order of 5 meters and the maximum velocity of the order of 30 m/s, in real units our choice of parameters corresponds to a 1-km domain and a time interval between measurements of 30 s.

The first set of experiments is performed measuring position and velocity of all the $N = 150$ cars. The experiments are relative to the time intervals

(a) $t \in [4 \times 10^4, 1.5 \times 10^5]$,
(b) $t \in [7.2 \times 10^5, 9 \times 10^5]$,
(c) $t \in [2 \times 10^7, 2.2 \times 10^7]$,

already shown in Fig. 1. A time interval of 1 corresponds to 1/6 s in real units.

One of the main results of Ref. [35] is that in chaotic systems, the long time limit of the number of eigenvalues of the analysis covariance matrix $\mathbf{P}^a$ greater than zero is equal to the number of null and positive Lyapunov exponents obtained through the algorithm of Ref. [44]. In the present work, we are dealing with a nonchaotic algorithm showing a very slow transient behavior that only for $t > 10^7$ leads to the asymptotic number of nonnegative Lyapunov exponents. We show that in the three time intervals, (a), (b), (c), the number of positive eigenvalues of $\mathbf{P}^a$ (and consequently the number of perturbations m needed to perform assimilation in the EKF-AUS algorithm) is equal to the number of positive Lyapunov exponents as calculated with the Ref. [44] algorithm up to the initial time of the three different intervals. Indeed, in Fig. 3 relative to the time interval labeled as (a), the number of the $\mathbf{P}^a$ eigenvalues significantly greater than zero is 8 and is equal to the number of positive exponents in the same interval. In interval (b) the number of still positive Lyapunov exponents is 4 like the number of positive eigenvalues shown in Fig. 4. Finally, in Fig. 5 the number of positive eigenvalues of $\mathbf{P}^a$ is two (the third one is rapidly decaying to zero) as is the number of positive exponents in interval (c).

These results show that in a nonchaotic system there is an agreement between the algorithm of Ref. [44] and EKF-AUS in the sense that the number of null and positive Lyapunov exponents is equal to the number of positive eigenvalues of $\mathbf{P}^a$. Indeed, we observe that also during the transient behavior from the uniform unstable state, there is the same agreement

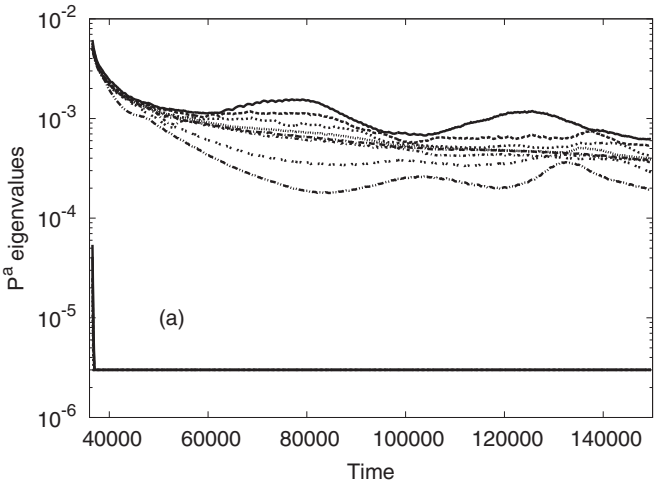

FIG. 3. $\mathbf{P}^a$ eigenvalues as a function of time in the assimilation experiment performed in the time interval (a) using the EKF-AUS algorithm run with $m = 13$, $\sigma_0 = 10^{-2}$, $\tau = 180$, $p = 150$ (all cars monitored).

provided that we consider the Lyapunov exponents calculated up to the time when we are performing the assimilation.

It is important to notice that this equivalence holds in the limit of linear evolution of the small perturbations around the *truth* trajectory. As already pointed out in Ref. [35], when the distance in phase-space between the *truth* and the *analysis* is not so small, some nonlinear effects become important. One way to solve this problem is to run the EKF-AUS algorithm with a number of perturbations m slightly larger than the exact number of null and positive Lyapunov exponents. In Fig. 6, we show in the time interval (b) what happens if we start with an *analysis* whose distance (the rms difference between states) from the *truth* is of the order of the measurement error ($\sigma_0 = 10^{-2}$). We see that in order to obtain the convergence toward the *truth*, we need at least $m = 6$. Nevertheless, we must notice that after the brief period of convergence (let us say when the error becomes smaller than 10^{-4}), the non-null

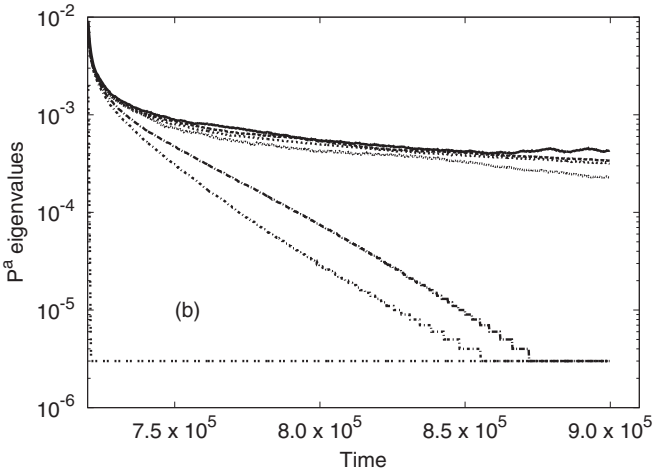

FIG. 4. $\mathbf{P}^a$ eigenvalues as a function of time in the assimilation experiment performed in the time interval (b) using the EKF-AUS algorithm run with $m = 8$, $\sigma_0 = 10^{-2}$, $\tau = 180$, $p = 150$ (all cars monitored).

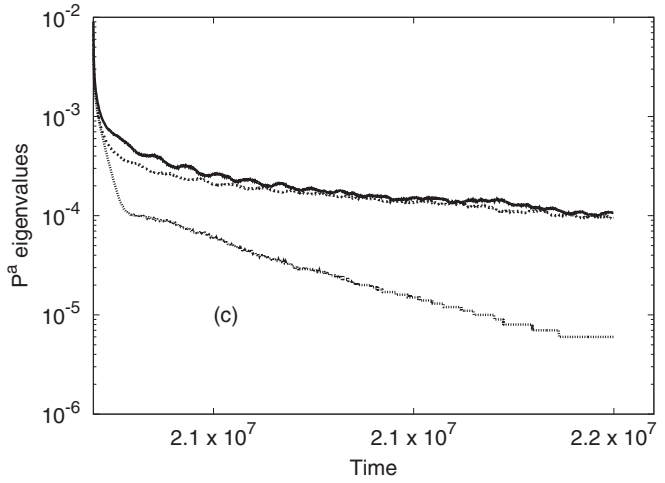

FIG. 5. $\mathbf{P}^a$ eigenvalues as a function of time in the assimilation experiment performed in the time interval (c) using the EKF-AUS algorithm run with $m = 5$, $\sigma_0 = 10^{-2}$, $\tau = 180$, $p = 150$ (all cars monitored).

eigenvalues of $\mathbf{P}^a$ become 4 as in the previous example and at this point one could safely run the EKF-AUS with $m = 4$ without the risk of filter divergence. In summary, we point out that in a practical implementation of the EKF-AUS one should use a number of perturbations somewhat larger than the theoretical value in order to obtain a "safer" filter.

From a practical point of view it is important to test if EKF-AUS is able to obtain convergence toward the *truth* trajectory also in the case when only a small fraction of the cars are monitored. Indeed, at the moment all the monitoring systems, both based on mobile-phone or on fixed GPS systems mounted by Insurance companies, involve only a small amount of cars. In the following, we show that the EKF-AUS algorithm is able to obtain the convergence toward the *truth* trajectory also when the number of monitored cars $p \ll N$.

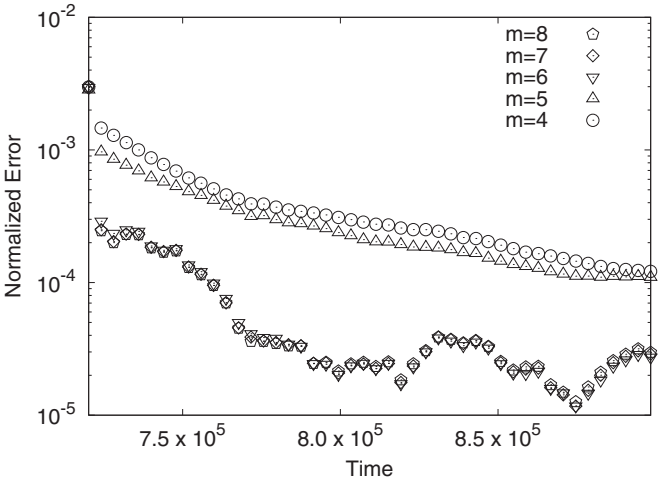

FIG. 6. Time evolution of the error (the rms difference between the *truth* and the *analysis* states normalized by the number of degrees of freedom, $2N$) during the assimilation performed in the time interval (b) for $m = 8,7,6,5,4$. Error values relative to $m = 6,7,8$ are so similar that they cannot be distinguished in the figure.

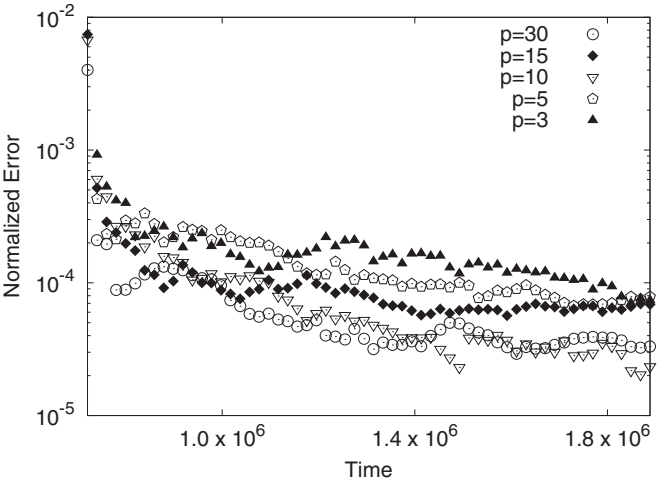

FIG. 7. Time evolution of the error (the rms difference between the *truth* and the *analysis* states normalized by the number of degrees of freedom, $2N$) during the assimilation performed in the time interval (b) for $m = 6$ and for different values of the number of monitored cars $p = 30,15,10,5,3$.

The results of the experiments that are most significant for traffic applications are shown in Fig. 7 that illustrates the performance of the filter for $p = 30,15,10,5,3$ in the time interval labeled as (b). As the reader can see in all cases, the convergence is very good and quite independent of the number of monitored cars. Moreover, the analysis error is considerably smaller than the observation error $\sigma_0 = 10^{-2}$. This is due to the fact that in the stop and go situations, the correlation of the velocity among the cars within each group is very high, so that it is enough to monitor a small fraction of cars to obtain the convergence. The simulation shown is performed with $m = 6$. Similar results (not shown) are obtained in the other two time intervals.

VI. CONCLUSIONS

The development of new observation scenarios motivated the application of advanced data assimilation techniques to traffic dynamic models, as the use of these techniques enhance the accuracy in the estimate of traffic flow. The results of the idealized study presented here are encouraging and, thus, open a pathway to real-world applications and effective traffic control. The EKF-AUS algorithm used here was developed for chaotic systems and is based on a dynamic approach that greatly reduces the computational cost of the full EKF. This is accomplished by restricting the matrix computations to the relevant degrees of freedom, which correspond to the number of unstable and neutral directions of the tangent space. In the present context of the OV model of traffic flow, the dynamics is not chaotic, so that the only directions that are relevant for the performance of the algorithm are those associated with zero exponents.

The result is that the algorithm is not only suitable for the application to a nonchaotic model, but it is even more efficient because it must account for a very small number of directions. This result is important for both theoretical and applicative reasons. From a theoretical point of view, we have shown that also in a nonchaotic system there is a strong equivalence between

the EKF-AUS algorithm and the algorithm used to compute the Lyapunov exponents and vectors [44]. This finding confirms the important relation there is between the linear stability behavior of a dynamical system and the data assimilation algorithm to be used to keep track of its trajectories.

From a practical point of view we have shown that the EKF-AUS algorithm, with a computational burden much lower than that of the full EKF algorithm, is able to perform very accurate analysis for the OV model also in the case of a very small number of monitored cars. The major cut in computational cost comes from reducing the dimension m of $\mathbf{E}^f$ and $\mathbf{E}^a$ with respect to the standard Kalman filter by a factor $m/2N$ and using a number of monitored cars $p \ll N$. The main part of computational cost scales linearly in $m/2N$, while the inversion in Eq. (13) scales as $(p/N)^3$.

An additional result is the ability of the algorithm to estimate the neutral directions of the system, the only relevant directions where the errors can temporarily grow in the present case of a nonchaotic system. This is important because the structure of these modes indicates where errors can grow at a given time. Not surprisingly, the velocity components of these direction-vectors are concentrated in the narrow regions between stops and goes, where gradients are very sharp: correspondingly, these regions are the ones where also the errors in the estimate are largest and, therefore, are the regions where observations are monthly needed.

This confirms previous results obtained with different models and indicates that making special (adaptive) observations at locations where the unstable structure attains its maximum is an effective strategy to reduce the overall error [38,39]. This would mean, for traffic dynamics, to make a single observation near the critical transition between a stop and a go.

The present study paves the way to the possible use of this algorithm in real-time software for traffic monitoring and prediction. Nevertheless, it must be stressed that our approach is based on the perfect model scenario, i.e., on the assumption that the OV model equations perfectly describe the dynamics of the system. In real applications, one should face the problem of model error: the discrepancies between the actual evolution of the system and the evolution described by the model. It is still an open question how to insert the model error in the formalism of AUS assimilation and in particular the interplay between the stable, neutral, and unstable manifolds and the structure of the model error. This will be surely the topic of further research and a necessary preliminary step for the application of our results to traffic dynamics.

ACKNOWLEDGMENTS

This work has been supported by Progetto Pegasus Ind.2015. We thank G. Lacorata for useful discussions about the calculation of Lyapunov exponents.

[1] M. C. Gonzlez, C. A. Hidalgo, and A.-L. Barabasi, Nature (London) **453**, 779 (2008).
[2] L. Liu *et al.*, *Proceedings of the 12th International IEEE Conference on Intelligent Transportation Systems, St. Louis, MO, 2009* (IEEE, Piscataway, NJ, 2009), pp. 1–6.
[3] A. Bazzani, B. Giorgini, S. Rambaldi, R. Gallotti, and L. Giovannini, J. Stat. Mech.: Theory and Experiment (2010) P05001.
[4] A. Bazzani, B. Giorgini, R. Gallotti, L. Giovannini, M. Marchioni, and S. Rambaldi, *The Third IEEE International Conference on Social Computing, Boston, MA, 2011* (IEEE, Piscataway, NJ, 2011), pp. 1455–1459.
[5] A. Mazloumina, N. Geroliminis, and D. Helbing, Phil. Trans. R. Soc. A **368**, 4627 (2010).
[6] M. Treiber, A. Hennecke, and D. Helbing, Phys. Rev. E **62**, 1805 (2000).
[7] A. Bazzani, B. Giorgini, L. Giovannini, R. Gallotti, and S. Rambaldi, in *34th International Convention on Information and Communication Technology, Electronics and Microelectronics MIPRO, Opatija, Croatia*, edited by P. Biljanovic *et al.* (IEEE, Piscataway, NJ, 2011), pp. 1615–1618.
[8] A. H. Jazwinski, *Stochastic Processes and Filtering Theory* (Academic Press, New York, 1970).
[9] M. Bando, K. Hasebe, A. Nakayama, A. Shibata, and Y. Sugiyama, Phys. Rev. E **51**, 1035 (1995); Jpn. J. Ind. Appl. Math. **11**, 202 (1994).
[10] M. Bando, K. Hasebe, K. Nakanishi, A. Nakayama, A. Shibata, and Y. Sugiyama, J. Physique I **5**, 1389 (1995).
[11] D. Helbing, Rev. Mod. Phys. **73**, 1067 (2001).
[12] M. Treiber and A. Kesting, *Traffic Flow Dynamics* (Springer-Verlag, Berlin Heidelberg, 2013).
[13] K. Nakanishi, K. Itoh, Y. Igarashi, and M. Bando, Phys. Rev. E **55**, 6519 (1997).
[14] G. Orosz, B. Krauskopf, and R. E. Wilson, Physica D **211**, 277 (2005).
[15] A. Trevisan and F. Pancotti, J. Atmos. Sci. **55**, 390 (1998).
[16] M. Papageorgiou, *Applications of Automatic Control Concepts to Traffic Flow Modeling and Control* (Springer-Verlag, New York, 1983).
[17] R. E. Kalman and R. S. Bucy, J. Basic Eng. **83**, 95 (1961).
[18] D. C. Gazis and C. H. Knapp, Transp. Sci. 1971 **5**, 283 (1971).
[19] H. M. Sendula and C. H. Knapp, *Proceedings of the 1972 International Conference on Cybernetics and Society, Washington, DC* (IEEE, Piscataway, NJ, 1972), pp. 469–472.
[20] M. W. Szeto and D. C. Gazis, Transp. Sci. **6**, 419 (1972).
[21] N. E. Nahi and A. N. Trivedi, Transp. Sci. **7**, 269 (1973).
[22] N. E. Nahi, Proc. IEEE **61**, 537 (1973).
[23] S. A. Smulders, in *Proceedings of the 10th International Symposium on Transportation and Traffic Theory* (Elsevier, New York, 1987).
[24] N. Bhouri, H. Hadj-Salem, M. Papageorgiou, and J. M. Blosseville, Traffic Eng. Control **29**, 579 (1988).
[25] M. Cremer, *Flow Variables: Estimation Concise Encyclopedia of Traffic and Transportation Systems* (Pergamon Press, London, 1991), pp. 143–148.
[26] M. Cremer, *Der Verkehrsablauf auf Schnellstrassen* (Springer-Verlag, Berlin 1979).
[27] M. Cremer, M. Papageorgiou, and G. Schmidt, Forschung Strassenbau und Strassenverkehrstechnik **307**, 1 (1980).
[28] R. R. Kohan and S. A. Bortoff, Proceedings of the 37th IEEE Conference on Decision and Control **1**, 1012 (1998).

[29] J. Meier and H. Wehlan, *IEEE Proceedings on Intelligent Transportation Systems, Oakland, CA, 2001* (IEEE, Piscataway, NJ, 2001), pp. 440–445.
[30] C. P. I. J. Van Hinsbergen, T. Schreiter, F. S. Zuurbier, J. W. C. van Lint, and H. J. van Zuylen, IEEE T. Intell. Transp. **13**, 385 (2012).
[31] Y. Wang and M. Papageorgiou, Transportation Res. B **39**, 141 (2005).
[32] I. Okutani and Y. J. Stephanedes, Transp. Res. B **18**, 1 (1984).
[33] F. X. Le Dimet and O. Talagrand, Tellus A **38/2**, 97 (1986).
[34] A. Trevisan, M. D'Isidoro, and O. Talagrand, Q. J. Roy. Meteor. Soc. **136**, 487 (2010).
[35] A. Trevisan and L. Palatella, Nonlin. Proc. Geophys. **18**, 243 (2011).
[36] A. Trevisan and L. Palatella, Int. J. Bifurcation Chaos **21**, 3389 (2011).
[37] L. Palatella, A. Carrassi, and A. Trevisan, J. Phys. A: Math. Theor. **46**, 254020 (2013).
[38] A. Trevisan and F. Uboldi, J. Atmos. Sci. **61**, 103 (2004).
[39] F. Uboldi and A. Trevisan, Nonlin. Proc. Geophys. **16**, 67 (2006).
[40] A. Bazzani and S. Rambaldi, personal communication (2011).
[41] J. P. Eckmann and D. Ruelle, Rev. Mod. Phys. **57/3**, 617 (1985).
[42] F. Ginelli, P. Poggi, A. Turchi, H. Chaté, R. Livi, and A. Politi, Phys. Rev. Lett. **99**, 130601 (2007).
[43] P. V. Kuptsov and U. Parlitz, J. Nonlinear Sci. **22**, 727 (2012).
[44] G. Benettin, L. Galgani, A. Giorgilli, and J. M. Strelcyn, Meccanica **15**, 9 (1980); **15**, 21 (1980).